RUSSIAN JOURNAL OF EARTH SCIENCES, VOL. 3, NO. 1, PAGES 59–78, MARCH 2001

Computer technologies used to obtain new information on crustal structure in oceanic fracture zones: A case study on the active segment of São Paulo Fracture Zone, Central Atlantic

A. O. Mazarovich, S. Yu. Sokolov, G. V. Agapova, K. O. Dobrolyubova, and V. N. Efimov

Geological Institute, Russian Academy of Sciences (GIN RAS)

Abstract. The paper deals with the possibility of obtaining innovative scientific information based on computer processing of data for a well-known area, the active segment of the São Paulo Fracture Zone (FZ), Central Atlantic, by means of digitizing a bathymetric map and an isopach map of sedimentary cover and supplementing the resultant mathematical models with satellite altimetry data. Our in-depth interpretation of the data resulted in the detection of structural heterogeneities in the rift zones and active segments of the fracture zones, of a tract of sedimentary cover that shows evidence of several deformation phases, and of previously unreported volcanic edifices. In addition, a system of NW-SE trending strike-slip faults was established. The study shows that converting information from paper carriers to a digital format and combining the results with Internet resources and deep sea sampling data creates an entirely new dataset amenable to state-of-the-art processing techniques eventually leading to unexpected corollaries.

Introduction

Over the past four decades, Soviet research vessels (R/Vs) collected in the world ocean outside economic zones a vast amount of non-digital materials of a great scientific value, which are now stored in a number of archives in the form of echo sounder records, seismic tapes on electrochemical paper, original map compilations, etc. On the other hand, for the past ten or fifteen years, the bulk of geological and geophysical information has been recorded and stored in a digital format. This virtually obviates merging the old and new data and analyzing them jointly. Therefore, the results of these surveys, whose costs amounted to astronomical figures, remain unavailable to scientific and applied usage. The recent explosion of information and, primarily, the advent of Internet call imperatively for digitizing the entire deep sea information collected by Soviet research vessels in order to enable its analysis by means of up-to-date techniques. This work is bound to lead to fundamentally new theoretical and applied conclusions regarding the structure and geodynamic evolution of the oceanic lithosphere.

The team of the Laboratory of Geomorphology and Ocean Floor Tectonics of the Geological Institute, Russian Academy of Sciences, has been using computer technologies since 1991. We have acquired and arranged extensive data for the Atlantic Ocean and adjoining onshore regions in the fields of seafloor topography and geology along with the data from gravity, magnetic, and acoustic surveys. These data are now available as a series of various maps of the Central Atlantic (Figure 1) in a format accessible to any Internet user at *http://atlantic.tv-sign.ru*. This series portrays clearly the geological setting of all the survey areas, covered by 22 marine expeditions of the Geological Institute over 15 years of its research in fundamental issues. We also designed a project to construct large-scale geological and geophysical maps elucidating comprehensively the setup of each survey area. This work involves creating a GIS for the Central Atlantic that would allow a quick access to data on any geographically positioned feature in this region. Our work, intended to assess the feasibility of obtaining fundamentally new scientific

Paper number TJE01055.
CCC: 0000–0000/2001/0301–0055$18.00

The online version of this paper was published July 24, 2001.
URL: http://rjes.agu.org/v03/TJE01055/TJE01055.htm
Print companion will be issued.

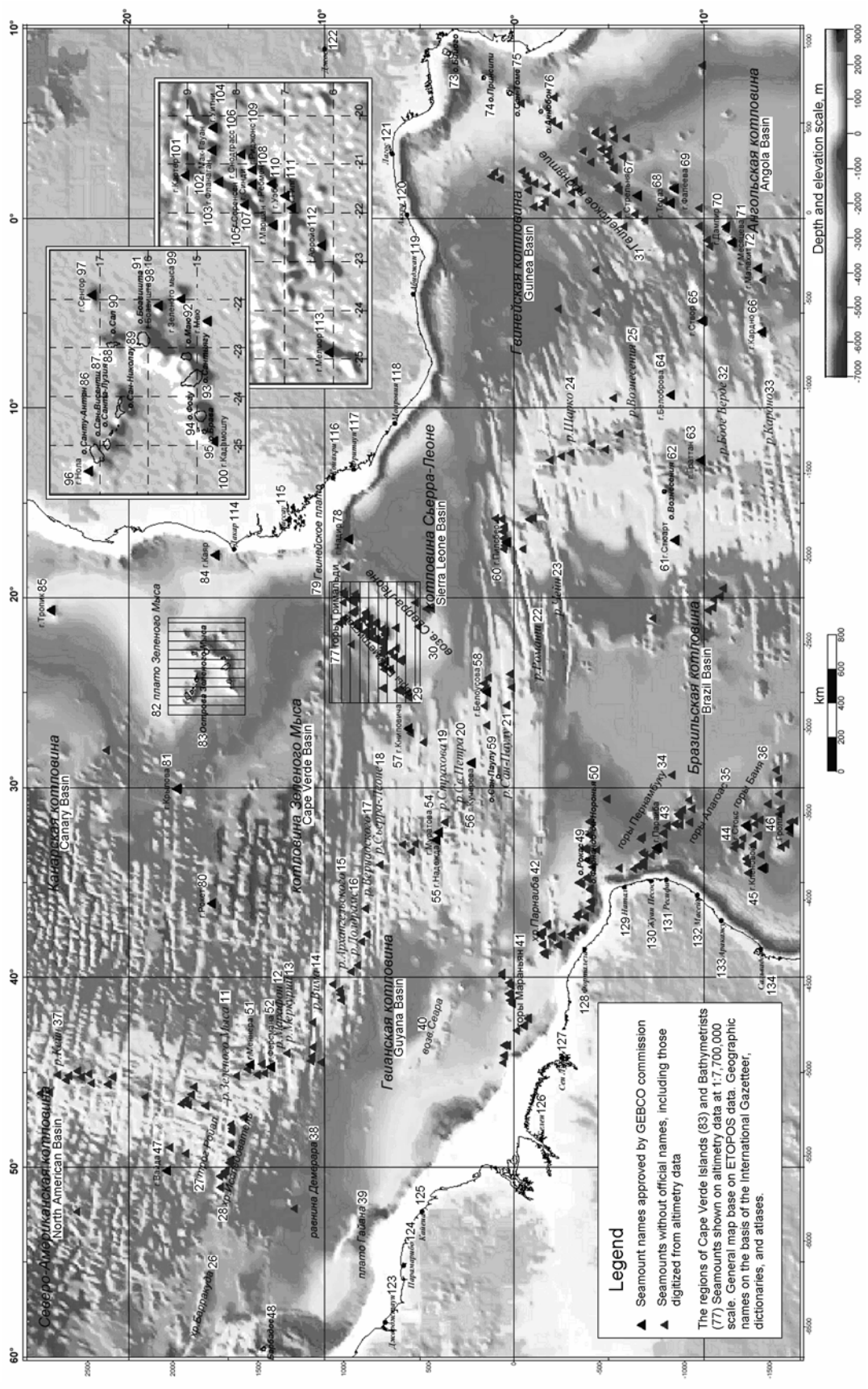
Legend
Seamount names approved by GEBCO commission
Seamounts without official names, including those digitized from altimetry data
The regions of Cape Verde Islands (83) and Bathymetrists (77) Seamounts shown on altimetry data at 1:7,700,000 scale. General map base on ETOPOS data. Geographic names on the basis of the International Gazetteer, dictionaries, and atlases.
Depth and elevation scale, m
km
Северо-Американская котловина
North American Basin
Канарская котловина
Canary Basin
котловина Зеленого Мыса
Cape Verde Basin
Гвианская котловина
Guyana Basin
Гвинейская котловина
Guinea Basin
котловина Сьерра-Леоне
Sierra Leone Basin
Бразильская котловина
Brazil Basin
Ангольская котловина
Angola Basin
плато Зеленого Мыса
плато Гвиана
равнина Демерара
Гвинейское плато
горы Пернамбуку
горы Алагоас
горы Бахия

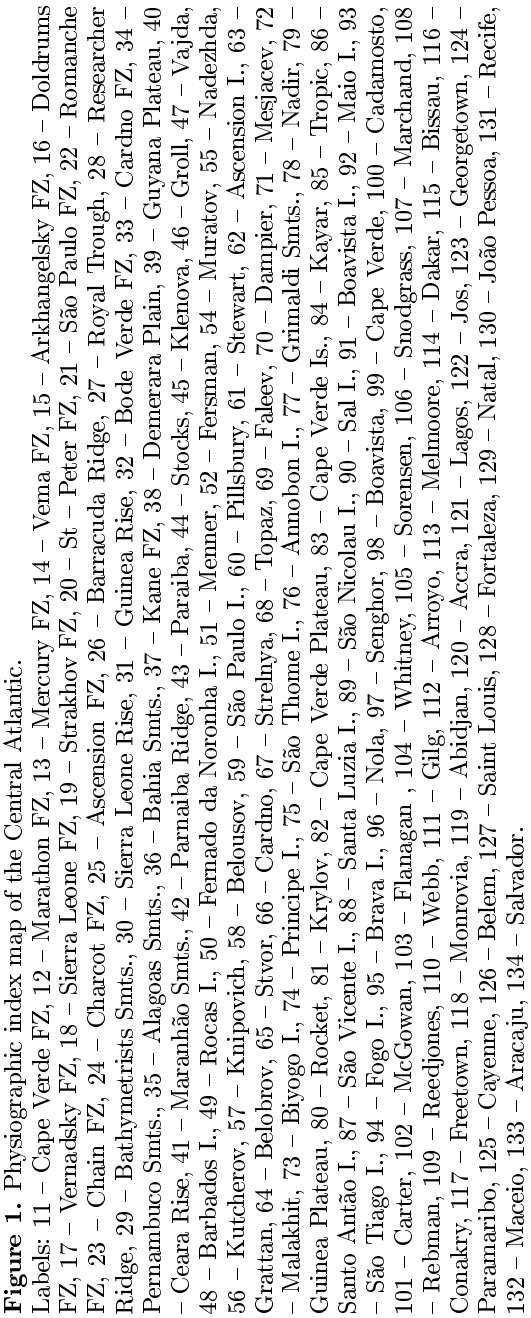

Figure 1. Physiographic index map of the Central Atlantic.
Labels: 11 – Cape Verde FZ, 12 – Marathon FZ, 13 – Mercury FZ, 14 – Vema FZ, 15 – Arkhangelsky FZ, 16 – Doldrums FZ, 17 – Vernadsky FZ, 18 – Sierra Leone FZ, 19 – Strakhov FZ, 20 – St – Peter FZ, 21 – São Paulo FZ, 22 – Romanche FZ, 23 – Chain FZ, 24 – Charcot FZ, 25 – Ascension FZ, 26 – Barracuda Ridge, 27 – Royal Trough, 28 – Researcher Ridge, 29 – Bathymetrists Smts., 30 – Sierra Leone Rise, 31 – Guinea Rise, 32 – Bode Verde FZ, 33 – Cardno FZ, 34 – Pernambuco Smts., 35 – Alagoas Smts., 36 – Bahia Smts., 37 – Kane FZ, 38 – Demerara Plain, 39 – Guyana Plateau, 40 – Ceara Rise, 41 – Maranhão Smts., 42 – Parnaiba Ridge, 43 – Paraiba, 44 – Stocks, 45 – Klenova, 46 – Groll, 47 – Vajda, 48 – Barbados I., 49 – Rocas I., 50 – Fernado da Noronha I., 51 – Menmer, 52 – Fersman, 54 – Muratov, 55 – Nadezhda, 56 – Kutcherov, 57 – Knipovich, 58 – Belousov, 59 – São Paulo I., 60 – Pillsbury, 61 – Stewart, 62 – Ascension I., 63 – Grattan, 64 – Belobrov, 65 – Stvor, 66 – Cardno, 67 – Strelnya, 68 – Topaz, 69 – Faleev, 70 – Dampier, 71 – Mesjacev, 72 – Malakhit, 73 – Biyogo I., 74 – Principe I., 75 – São Thome I., 76 – Annobon I., 77 – Grimaldi Smts., 78 – Nadir, 79 – Guinea Plateau, 80 – Rocket, 81 – Krylov, 82 – Cape Verde Plateau, 83 – Cape Verde Is., 84 – Kayar, 85 – Tropic, 86 – Santo Antão I., 87 – São Vicente I., 88 – Santa Luzia I., 89 – São Nicolau I., 90 – Sal I., 91 – Boavista I., 92 – Maio I., 93 – São Tiago I., 94 – Fogo I., 95 – Brava I., 96 – Nola, 97 – Senghor, 98 – Boavista, 99 – Cape Verde, 100 – Cadamosto, 101 – Carter, 102 – McGowan, 103 – Flanagan , 104 – Whitney, 105 – Sorensen, 106 – Snodgrass, 107 – Marchand, 108 – Rebman, 109 – Reedjones, 110 – Webb, 111 – Gilg, 112 – Arroyo, 113 – Melmoore, 114 – Dakar, 115 – Bissau, 116 – Conakry, 117 – Freetown, 118 – Monrovia, 119 – Abidjan, 120 – Accra, 121 – Lagos, 122 – Jos, 123 – Georgetown, 124 – Paramaribo, 125 – Cayenne, 126 – Belem, 127 – Saint Louis, 128 – Fortaleza, 129 – Natal, 130 – João Pessoa, 131 – Recife, 132 – Maceio, 133 – Aracaju, 134 – Salvador.

information through computer processing of data for a well-understood area, began with a survey area located over the active segment of the São Paulo Fracture Zone.

Previous Studies on the Active Segment of the São Paulo FZ

The São Paulo FZ extends, between the equator and 1° to 2°N, from the Amazon fan to the West African coast (Figure 2). According to GEODAS (Marine Trackline Geophysical Data CD. NOAA), this area was covered on 116 cruises by research vessels from USA, France, Germany, and USSR. From South America to 30°W, the fracture zone trends roughly E-W and is defined by marked topographic highs with intervening seafloor depressions totaling a width of ca. 100 km. At 30°W, the fracture zone swings northeast (Figure 2) and splays. As a result, its active segment between 25° and 30°W is structurally the most complex [*Agapova,* 1993; *Gorini,* 1981], and it was explored by a number of expeditions (Table 1). Four troughs of various lengths are recognized there. The eastern portions of the São Paulo FZ provide a southern boundary to the Sierra Leone Basin.

The mentioned expeditions acquired bathymetric data using both single-beam and multibeam echo sounders of various types, data on the structure of sedimentary cover from continuous seismic profiling, etc. The study area was sampled by piston cores of various types and dredging. We possess data for a total of 25 stations, of which 16 yielded assorted bedrocks, 3 yielded sedimentary rocks, and the remaining 6 were barren. In the north of the study area, undersea photographs were taken on Cruise 7 of the R/V Akademik Nikolaj Strakhov. In addition, in 1997, in the central part of the survey area, the French submersible Nadir collected information at 62 stations [*R. Hekinian,* personal communication, May 17, 2000].

On Cruise 7 of the R/V Akademik Nikolaj Strakhov in 1988, a bathymetric survey was performed using an ECHOS-625 multibeam echo sounder on 23 tacks 5 nautical miles apart (Figure 3). The primary bathymetric map [*Agapova,* 1993] (Figure 4) is an original unprocessed map, 1:250,000 scale by the equator, with a contour interval of 100 m. A color version of this map was published [*Equatorial...,* 1997, p. 8]. The primary isopach map of sedimentary cover with a 200 m contour interval and the acoustic basement map at the same scale were published as well.

Digitizing the Maps and Constructing a Numerical Model

For the reader's convenience, the procedure of converting the mentioned cartographic information, which involves contour lines, to a digital format can be divided into two phases.

Phase 1 – Digitizing the data. The primary bathymetric map was scanned and its image saved in a raster format.

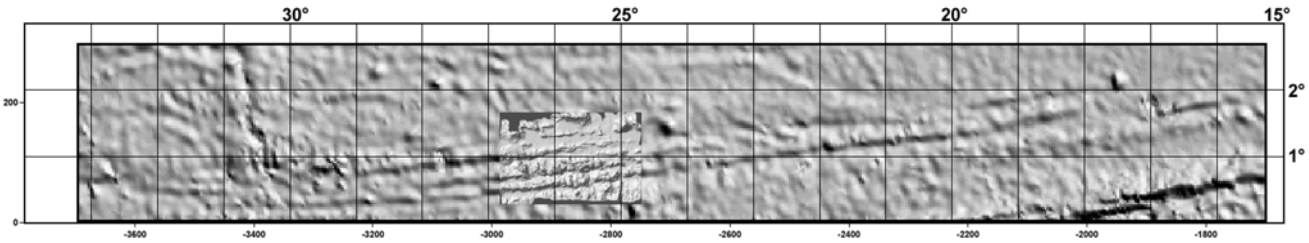

Figure 2. The São Paulo FZ and location of the detailed survey area covered on Cruise 7 of the R/V Akademik Nikolaj Strakhov (Geological Institute, Russian Academy of Sciences, 1988). Cartographic base, from satellite altimetry [*Smith and Sandwell,* 1997].

In scanning the map, our objective was to obtain as contrasting and clear an image as practicable and, if possible, in the black and white mode. Next, in a semi-automated mode (i.e., both by hand and by tracing image elements by contrast) and using vector graphics editors, the map was converted to a vector format, that is, depth contours and isopachs were imaged by a system of polylines with assigned depth and thickness values, respectively. Thus, a contour value can be saved as the name of a vector layer into which only objects pertaining to this particular value are placed.

Then, the reference frame for the vector images thus obtained was recalibrated from the conventional coordinates of the primary working map area to the real projection values. In this form, the information can already be used in GIS and geostatistical programs as a set of vector elements, although by no means as a spatial function represented uniformly (with a fixed discretization interval) over a certain region. After this, information is converted to the form of

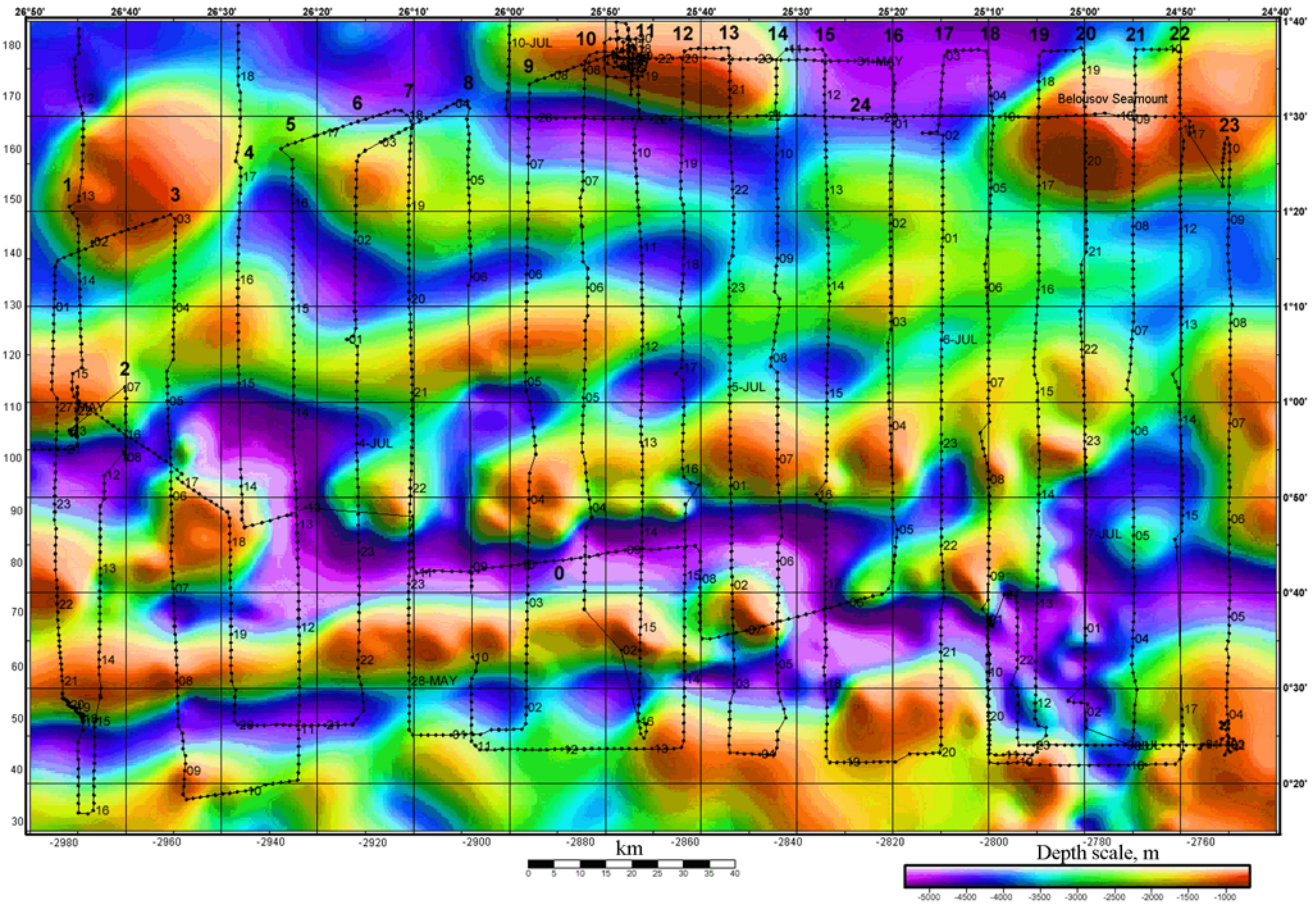

Figure 3. Track of the R/V Akademik Nikolaj Strakhov Cruise 7. Cartographic base, from predicted topography [*Smith and Sandwell,* 1997]. Large numerals (0, 1–24) label seismic profiles.

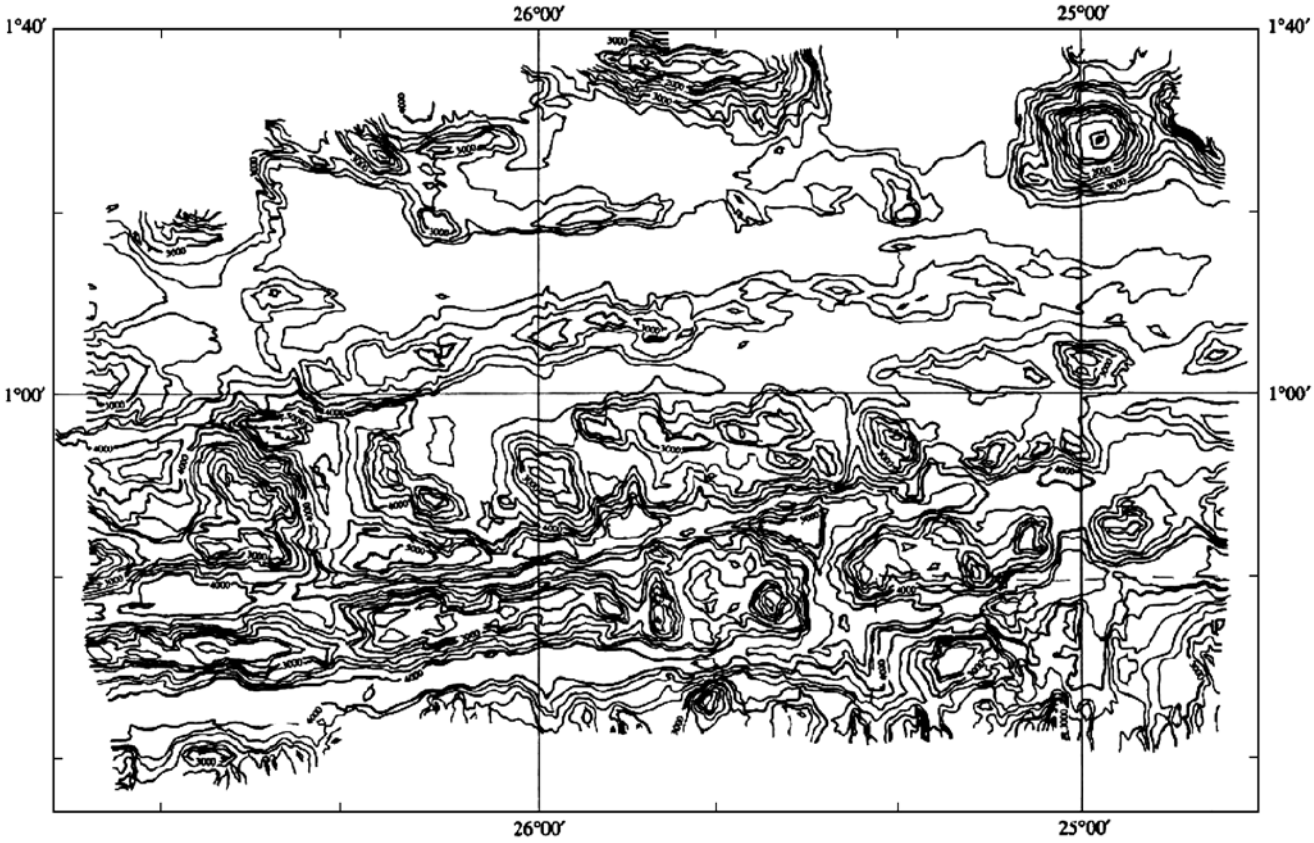

Figure 4. Primary bathymetric map [*Agapova,* 1993].

an XYZ point list describing the contour pattern, where each point is represented by three spatial values. The real coordinate vector format and the list format are end products after the digitizing phase. Note that Z value can stand for any parameter that provides the basis for a primary map, such as relief, sediment thickness, gravity, etc.

Phase 2 – Creating a numerical model. This phase involves the computation, using statistical methods, of the most probable values of the water depth (or any other parameter) for strictly determined points in the XYZ list of values. These points are the nodes of the regular spatial XY grid, whose dimension and interval are set depending on the degree of detail and the quality of the primary material and on the map scale. This procedure yields a set of Z values at the grid nodes referred to as a mathematical model computed from real life data, some nodes eventually remaining vacant. Irrespective of which statistical method was used for computation, the certainty of the model increases with the density of the map contours. Certainty is greater in areas with steeper slope gradients or rugged topography, that

Table 1. Information on expeditions that worked in the São Paulo survey area

Ship name	Cruise (Leg)	Year	Country
Challenger	No data	End of 19th century?	UK
Chain	CH63	1963	USA
Chain	CH03502	1963	USA
Atlantis II	AII020	1966	USA
Pillsbury	P6707	1967	USA
Robert Conrad	RC2806	1987	UK
Akademik Nikolaj Strakhov	07	1988	USSR
Akademik Nikolaj Strakhov	12	1991	USSR
Akademik Boris Petrov	17	1991	USSR
Akademik Nikolaj Strakhov	22	2000	Russia/Italy

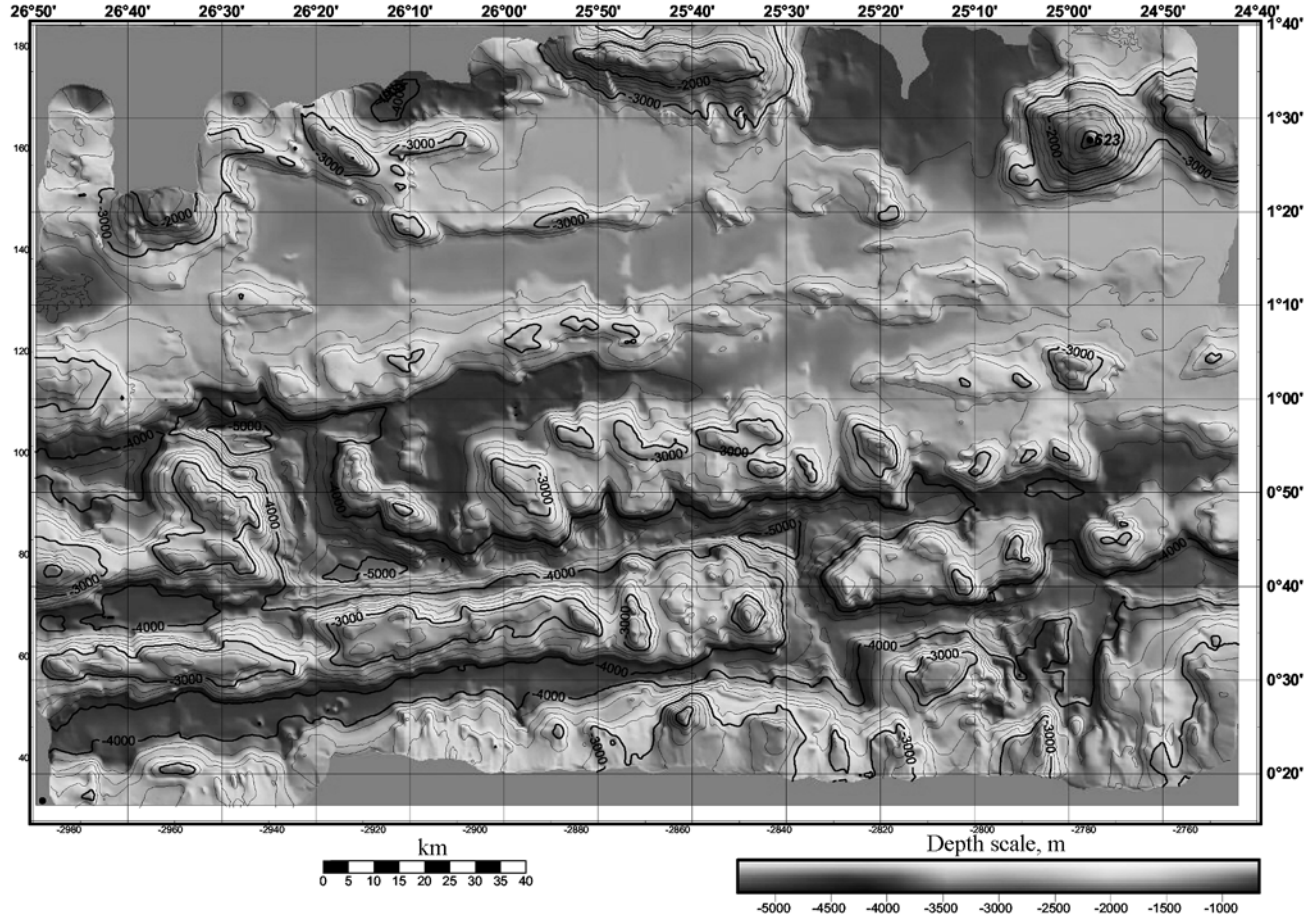

Figure 5. Bathymetric map of the active segment of the São Paulo FZ based on the data from Cruise 7 of the R/V Akademik Nikolaj Strakhov and Cruise 17 of the R/V Akademik Boris Petrov, constructed using the shaded relief technique. Contour interval 200 m.

is, where contour density was greater. Where the primary data density is insufficient – i.e., in the map areas over flat seafloor tracts with isobaths wide apart, the computation algorithms generate values that are poorly linked to reality. In this procedure, the criterion of a satisfactory certainty is the maximal coincidence of the contours constructed on the grid with the primary contours. Where this coincidence occurs, the numerical model can be deemed adequate to the primary data. Those grid nodes falling in-between the primary contours contain interpolated values of the parameter in question, which is as much as can be expected from models constructed on the basis of materials imaged in contour lines. As a last resort, to correct the model in those places where it was plainly inadequate to nature, but which were clear enough from the standpoint of human perception and experience, additional data were introduced by drawing extra isobaths (or isopachs), whose presence in the dataset ensured the stabilization of deviations in the functioning of the computation algorithms. This stabilization technique is quite admissible until the researcher has obtained new experimental data.

All the peculiarities just mentioned of the procedure used to obtain the numerical model and assess its quality only apply to materials represented by contours. In the modern echo sounding systems, in which the multibeam depth-measuring technique yields a vast array of XYZ points covering a seafloor band up to 3.5 times the water depth, the dataset obtained effectively approximates the status of a 3D function that encompasses the seafloor with an almost uniform discreteness – in other words, the status of a grid. In this situation, one should recur to alternative methods to visualize the seafloor, such as shaded relief, color or tinge coding (image map), and combinations thereof with the customary contour method, rather than the contour method in the pure state because, at the present-day degree of resolution, this method is more likely to conceal the information on seafloor relief than visualize it.

The predicted topography [*Smith and Sandwell,* 1997] fits well enough the shaded relief obtained through the digitization of the survey area (Figures 2, 5), although in places, especially over sediment-covered tracts, in the predicted topography initially separate features were merged together. To assess the accuracy of the predicted topography as compared to the real bathymetry, the two sets of contours were

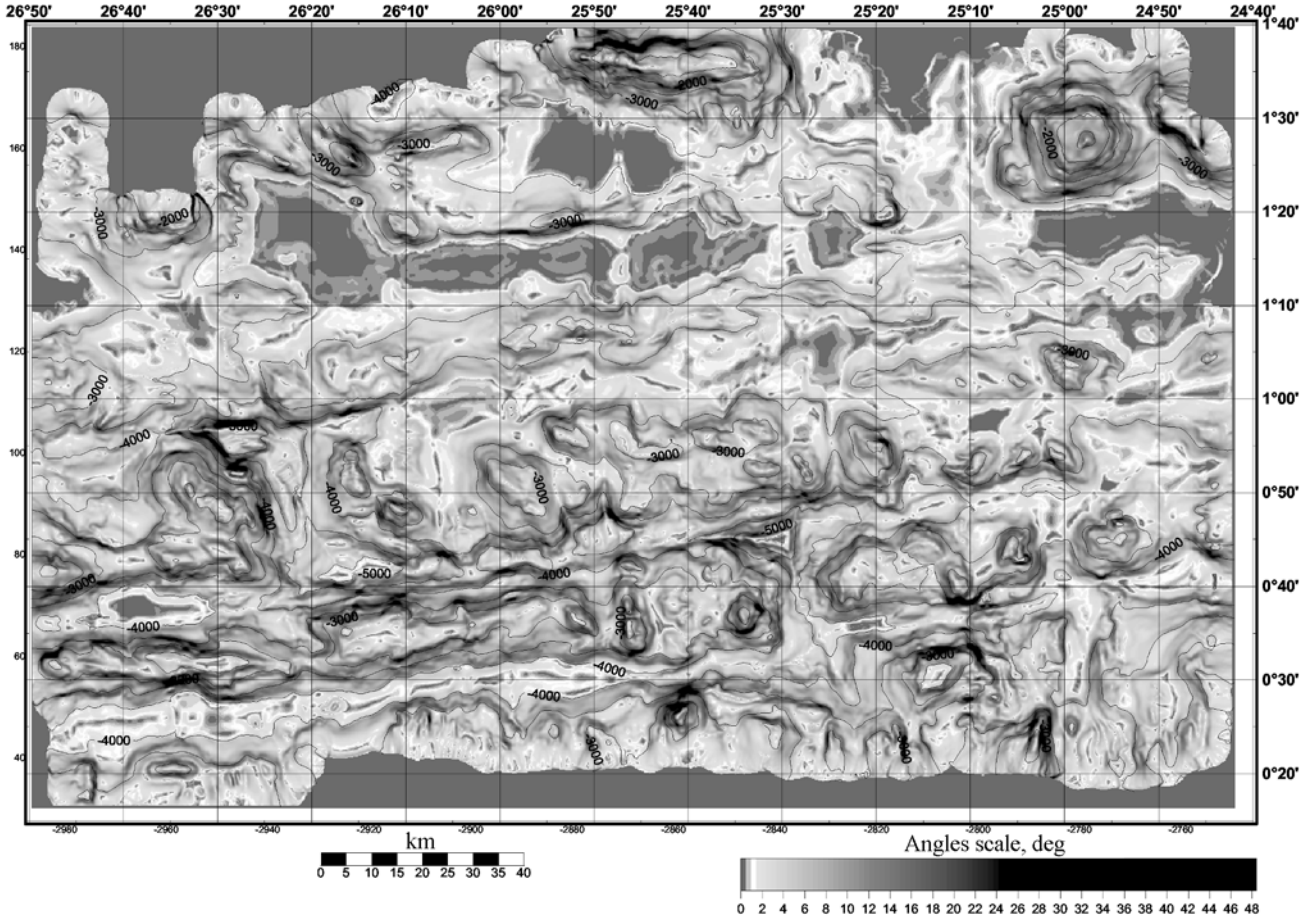

Figure 6. Slope angles map for the active segment of the São Paulo FZ. Contour interval 500 m.

superposed. The predicted topography was found to underestimate water depths with an error of ca. 100 m.

The gravity field over the survey area was imaged using satellite altimetry data [*Sandwell and Smith,* 1997] at a resolution of 1 arc minute. (Figure 9a). This field reflects sea surface elevations measures by the radar technique and recalculated to gravity values at the sea level, or free-air anomaly. Eighty to 90% of this anomaly is due to the influence of the topography, which causes the greatest density contrasts. The water/seafloor density contrast, equal to 1.72 g/sm^3, obscures the effects of crustal and mantle heterogeneities. Because the topography is surveyed by a different technique, echo sounding, whose results are fairly conclusive, in order to remove the obscuring influence of this interface the Bouguer anomaly was computed (Figure 9b). This anomaly reflects the gravity effects of crustal density heterogeneities and of the contrasting crust/mantle interface. Because at this interface density contrast is considerably smaller than within the overlying sequence, its contribution to the anomalous field must be expressed in gradual variations of the anomalous constituent. Crustal density heterogeneities cause high-amplitude Bouguer anomalies varying in sign relative to the general background.

To elucidate the distribution of rock assemblages, seafloor sampling data acquired by various ships were organized into computer tables in a relational database. Seismological data were additionally collected on Internet [*CNSS...,* 1997]. In general, we collected and systematized a large amount of factual materials enabling an exhaustive processing of the data. Baseline materials for our analysis were provided by a set of 1:650,000 maps, which we constructed:

Sheet 1. Index map of surveys on Cruise 7 of the R/V Akademik Nikolaj Strakhov (Geological Institute RAS, 1988) in the east of the active segment of the São Paulo FZ. S. Yu. Sokolov and V. N. Efimov (Figure 3).

Sheet 2. Topography of the active segment of the São Paulo FZ. G. V. Agapova and K. O. Dobrolyubov (Figure 5).

Sheet 3. Slope angles map over the active segment of the São Paulo FZ. K. O. Dobrolyubova, G. V. Agapova, and S. Yu. Sokolov (Figure 6).

Sheet 4. Isopach map of sedimentary cover over the active segment of the São Paulo FZ. V. N. Efimov, A. V. Kol'tsova (Vernadsky Institute of Geochemistry and Analytical Chemistry RAS), and S. Yu. Sokolov (Figure 7).

Sheet 5. Topography of acoustic basement of the active segment of the São Paulo FZ. S. Yu. Sokolov and V. N. Efimov (Figure 8).

Sheet 6. Gravity field over the active segment of the São

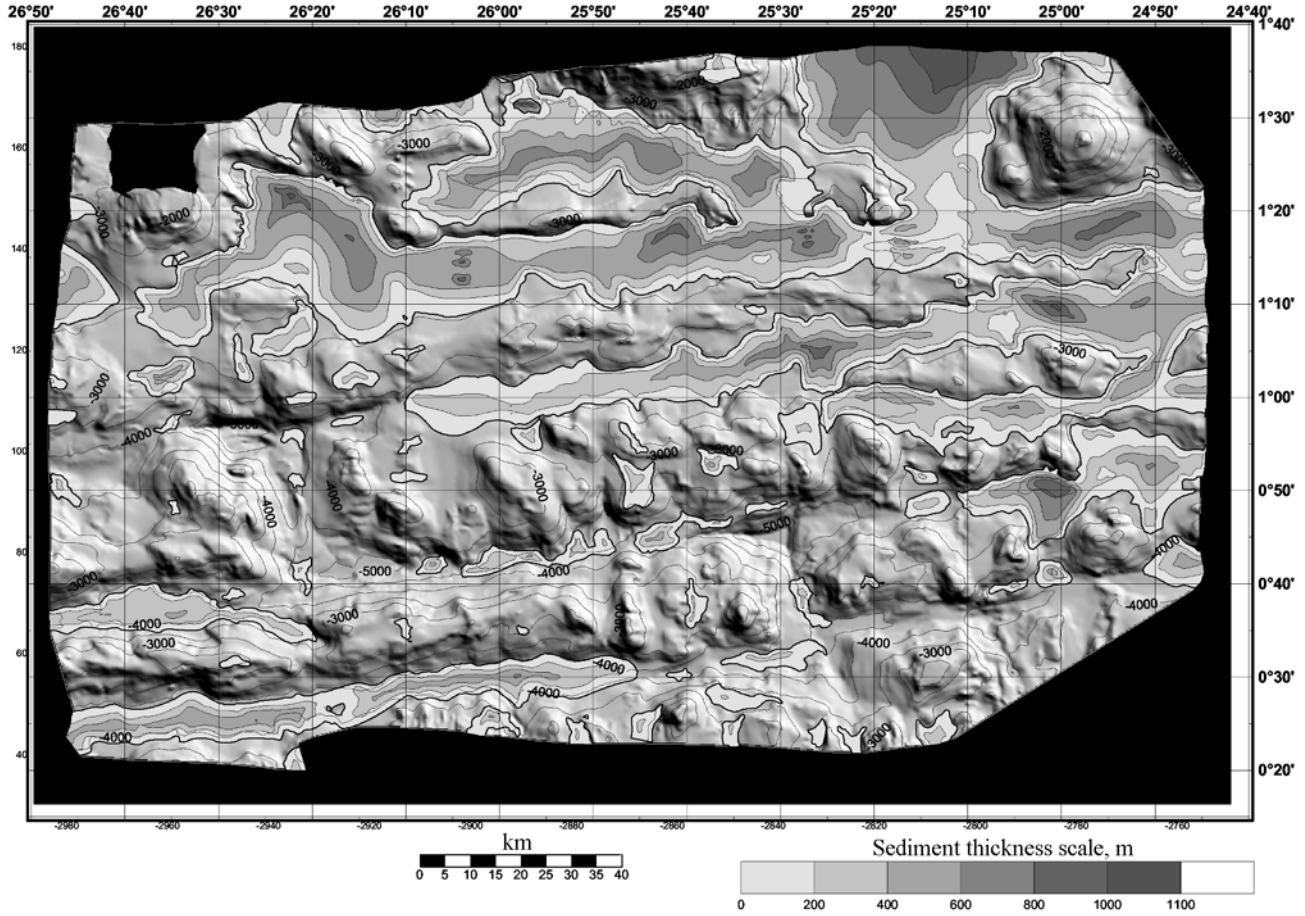

Figure 7. Isopach map of sedimentary cover over the active segment of the São Paulo FZ. Contour interval 500 m.

Paulo FZ. S. Yu. Sokolov (Figure 9).

Sheet 7. Seismicity of the active segment of the São Paulo FZ. S. Yu. Sokolov (Figure 10).

Sheet 8. Bedrock geology of the active segment of the São Paulo FZ. A. O. Mazarovich (Figure 11).

Principal Structural Peculiarities of the Active Segment of the São Paulo FZ: Results from the Integrated Analysis

The São Paulo FZ within the survey area consists of four roughly E-W trending troughs with intervening fracture-bounded rises (Figure 5). The troughs, as was reported earlier [*Agapova,* 1993], deepen from 3700 m b.s.l. in the north to 4200 m b.s.l. in the south. In addition, three rift valleys were established in the study area. In terms of geodynamic setup, the survey covered three active and four passive portions of transform faults and two seafloor spreading zones.

Because the São Paulo Fracture Zone represents a system integrating several closely spaced fractures covered by one and the same name, to discriminate between them we devised a virtual nomenclature that will be used hereinafter (Table 2, Figure 12).

The portion of the system under study is characterized by short rift segments and narrow alternating ridges.

The SP1 trough is the flank part of a fracture depression bounded on the north by a high ridge straddled by São Paulo I. and, within the survey area, by massive blocks whose tops occur in water depths less than 2000 m whereas, over Belousov Seamount, water depth is shallow as 623 m.

Along the north slope of the trough, a large flat ledge extends, whose surface lies in water depths of ca. 3500 m. Its edge is complicated by a narrow E-W trending ridge surmounted by peaks reaching shallower than 3000 m. Both on the ledge and in the SP1 trough, the most considerable sediment thicknesses are recorded, the sediment surface occupying the largest flat seafloor tracts within the survey area. This part of the trough, which lies more than 140 miles off São Paulo I., is the eastern flank portion of the largest strike-slip fault in the São Paulo fault system.

The SP1-2_W_RI ridge extends from the western limit of the study area nearly as far as its eastern boundary, decreasing gradually in width and height. All along the ridge, sediments are virtually absent. Its western part has the most rugged relief, displaying a mountain that reaches as

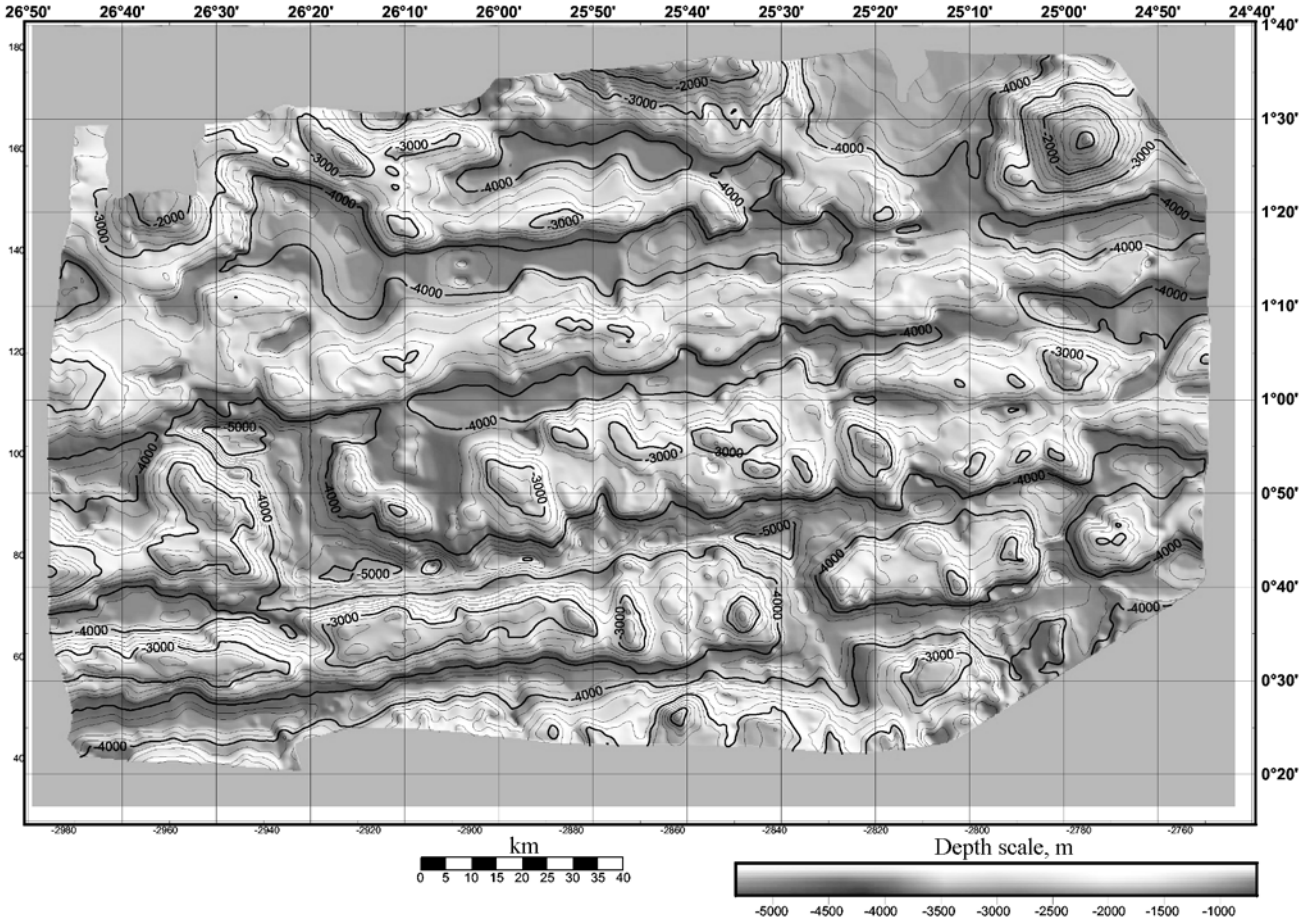

Figure 8. Topography of acoustic basement beneath the eastern part of the active segment of the São Paulo FZ. Contour interval 200 m.

shallow as ca. 2500 m b.s.l. East of it, a large bathymetric depression occurs on the continuation of the rift valley. It lies in water depths of 3400 to 3600 m and has gentle slope angles. From the western part of this depression, basalts were recovered (Figure 11). East of 26°25′ W, the crest of the ridge submerges as deep as 3200 m, individual peaks standing 200–400 m high over it. The ridge's axial part, especially on the east of the survey area, is characterized by repeated changes in the trend of its topographic features, which is particularly readily apparent from the slope angles map. In many places in the northeast of the area, seismic profiles across sedimentary cover (Figures 13a, 13b, 13c) depict flexures, normal faults, and homoclinal occurrence of strata. For this area, a strong uplifting of large portions of acoustic basement can be inferred.

The SP2 trough is expressed markedly in seafloor topography and corresponds to a depression in acoustic basement, whose eastern part is filled with sediments 200 to 1100 m thick. West of the rift, the trough passes into an irregularly shaped depression showing a mesh structure. In the trough, earthquake epicenters cluster (Figure 10). Eastward of the **NB_SP2_E** nodal basin (see below), the trough widens gradually. Along its axis, a stripe of flat seafloor extends intermittently, north and south of which slope angles become greater. Inside the trough, areas with steeper slopes are encountered. In places, the trough widens abruptly, forming depocenters with sediments 1000 to 1100 m thick.

The SP2-3_W_RI ridge, bounding the rift on the west, consists of two parts separated by a narrow NW-trending saddle. The southern, fracture-bounded part is a narrow, roughly E-W trending crest with two summits separated by a saddle. The western, rift-bounded part is an angular rise in water depths somewhat shallower than 2000 m. Its southern slope displays average angles of 8 to 12°, locally showing sharp, 20 to 45° scarps. The northern slope is more gentle.

The SP2-3_RI rift zone (26°25′ W) (Figure 14) is asymmetrical and has a steeper western slope with angles ranging chiefly from 12–15°, although locally exceeding 30°. Along the axis of the rift valley, a narrow ridge extends, which is up to 200 m high above the valley floor. Toward the north, the ridge becomes low and wide. Detailed bathymetry with 10–20 m contour interval shows the ridge to continue into the **NB_SP2_E** nodal basin, dividing it into two basins, northern and southern. This locality is distinguished by slope angles that are greatest in the entire survey

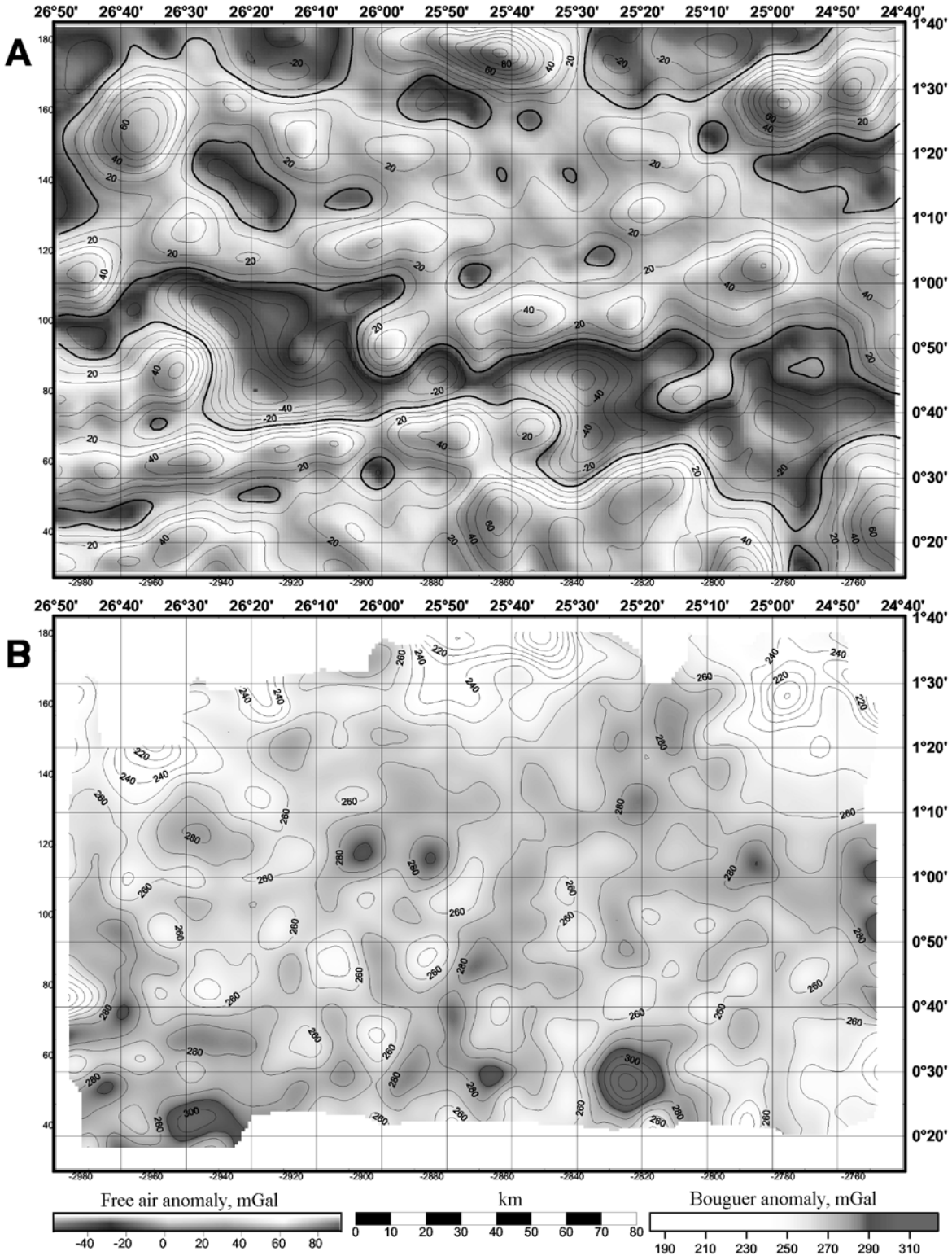

Figure 9. Gravity field over the active segment of the São Paulo FZ. A – free air anomaly; B – Bouguer anomaly.

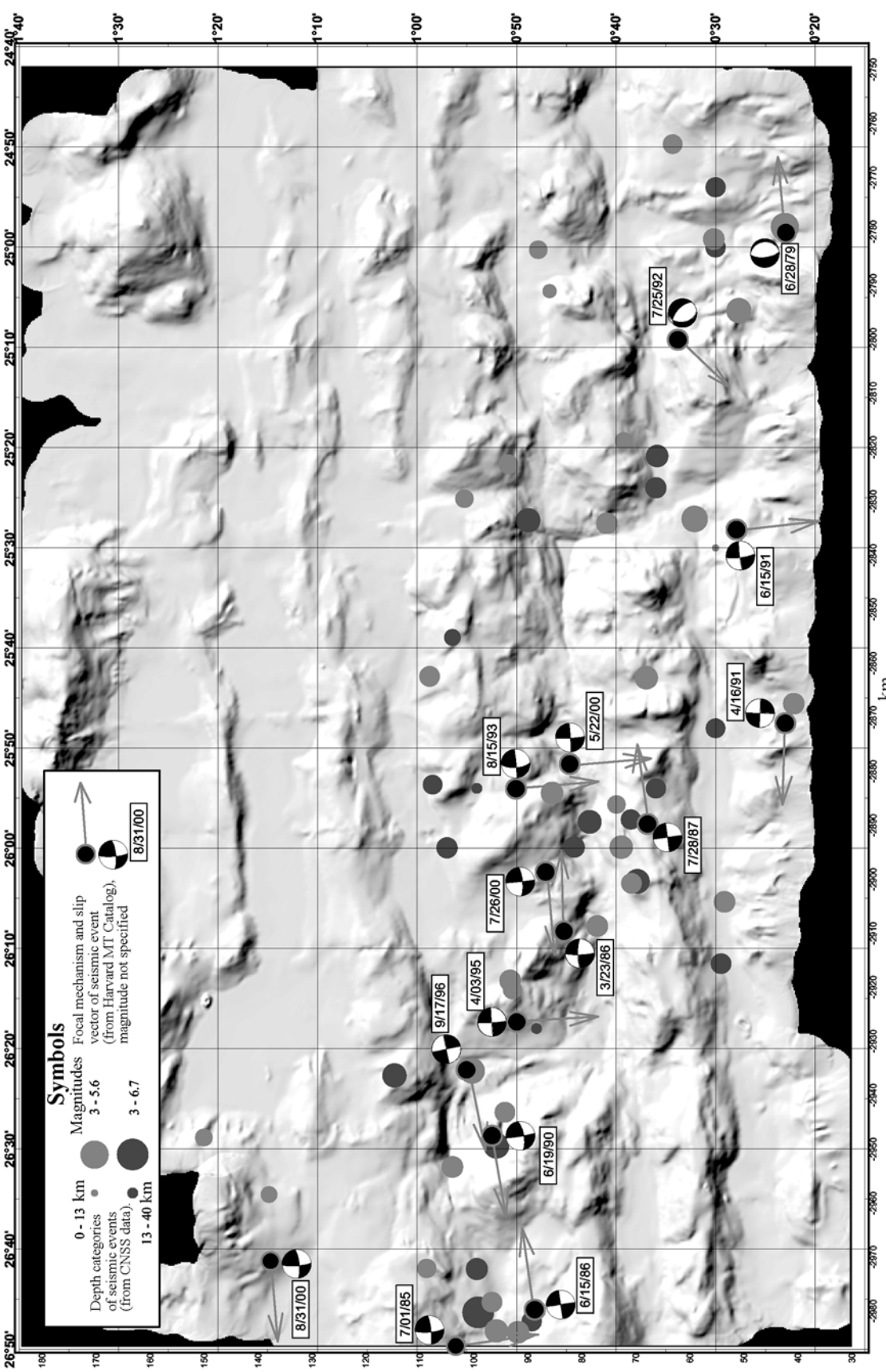

Figure 10. Seismicity of the active segment of the São Paulo FZ.

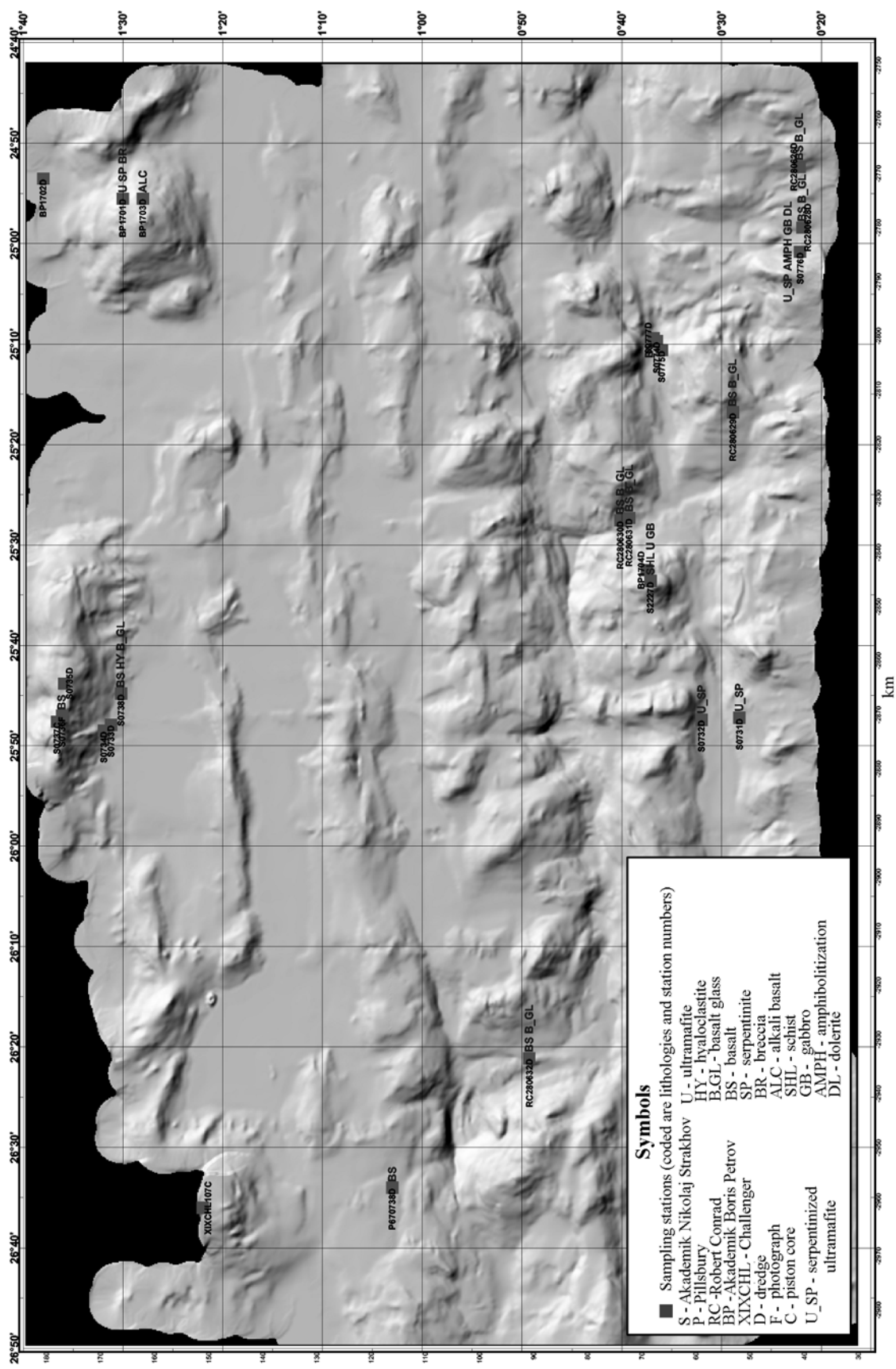

Figure 11. Bedrock geology of the active segment of the São Paulo FZ.

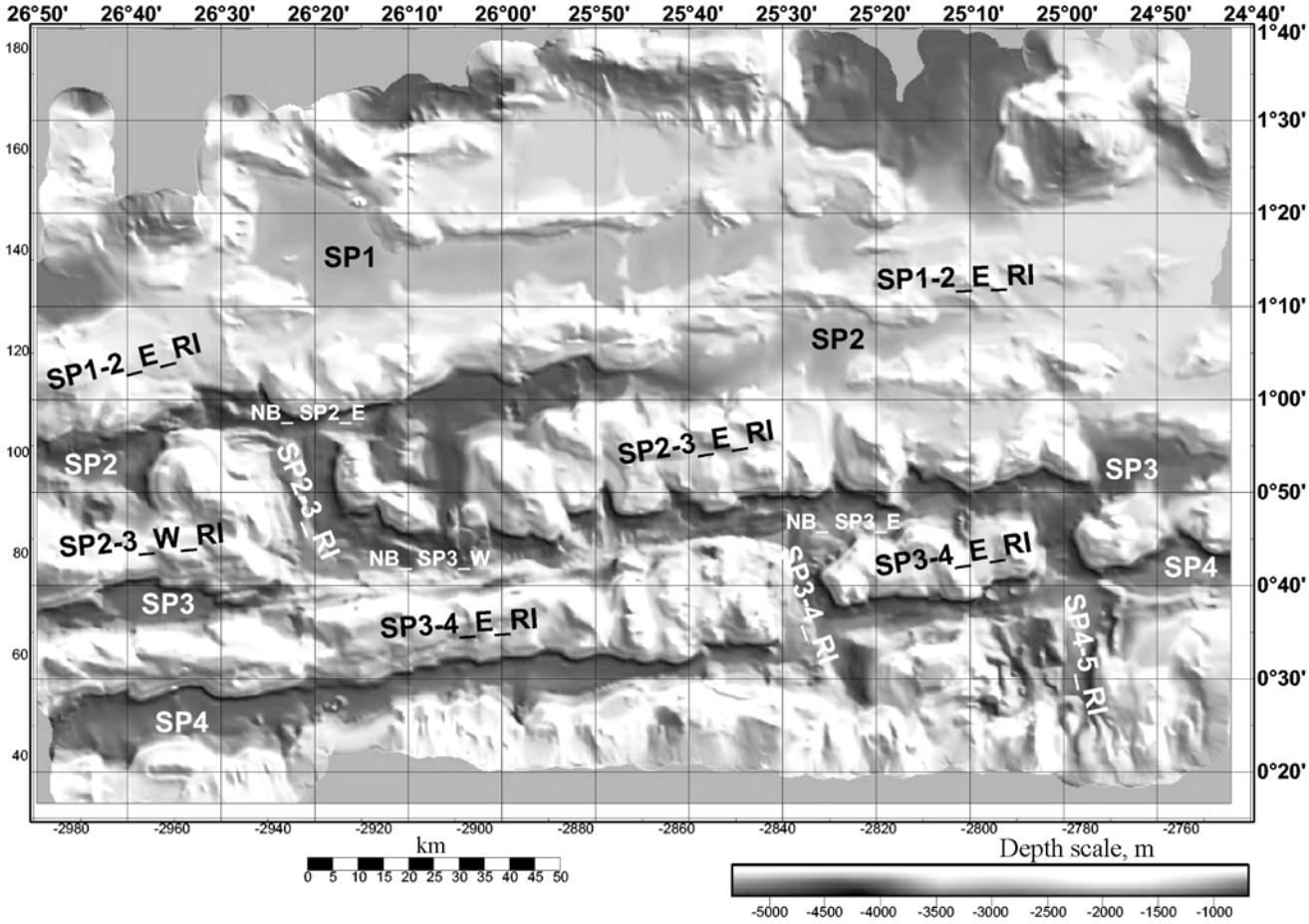

Figure 12. Schematic map showing virtual nomenclature for the active segment of the São Paulo FZ. For explanations, see Table 2.

area. In the southern part of the rift valley, the ridge turns gradually toward its western wall and finally merges with it. The ridge was sampled by dredge haul RC280632 from the R/V Robert Conrad [*Schilling et al.,* 1995], which recovered fresh basalt with glass. The ridge's tectonic setting and the rocks recovered render it interpretable as a neovolcanic rise. East and west of it, narrow and deep basins extend, the western being traceable into the **NB_SP2_W** nodal basin. The latter has gentle slopes with angles of a few degrees and a wide, flat bottom. This basin extends along the **SP2** fault.

The SP3 trough is well pronounced bathymetrically and corresponds to a depression in acoustic basement. Compared to the other basins, it has a scantier sediment fill, distributed sporadically, with average thicknesses of 200–400 m to zero over significant portions of the basin's western part. Sediments are thickest (1000–1100 m) in the eastern part of the fracture zone, where sediment-covered tracts are clearly manifest even in the active segment of the fault.

The SP2-3_E_RI ridge. The rift-bounded part of the ridge is a mountainous massif situated 2800 m b.s.l. The topography is dominated by large NW-trending mountains in water depths as shallow as 2000 m. The ridge has steep, in places up to 20°, slopes. Toward the east, the ridge lowers and widens, falling into several submerged mountains, finally to disappear at 25°W. This area is dominated by flat (up to 5°) surfaces representing tracts covered with sediment (Figure 7) as thick as 600 m. Further north, a low, short ridge with gentle (ca. 5°) slopes is recognized.

The SP3-4_W_RI ridge is virtually devoid of sedimentary cover throughout its length (Figure 7) and consists of two parts with dissimilar structures. The western, extending as far as ca. 25°55′ W, has a relatively flat top surface in water depths of up to 2600 m. The ridge is on the average 1500 m high and has slope angles ranging from 3 to 10°, in places up to 15° or even 30° (Figure 6). The most elevated part of the ridge displays a zone of flat surfaces with angles of 1.5 to 3° that can be interpreted as a fault zone. In plan view, it has an en echelon pattern with offsets of 3 to 4 km. Confined to these zones are NW-trending scarps suggestive of fault zones of the same trend and of a likely strike-slip character. The ridge slopes have average angles of 3 to 12°, which are in no way related to the ridge's attitude with respect to the active or passive parts of the transform faults. Both the southern and northern slopes display ledges with flat surfaces separated by steep (12–15°) scarps. Some of them are over 15 km long and as wide as 3 km. Unfortu-

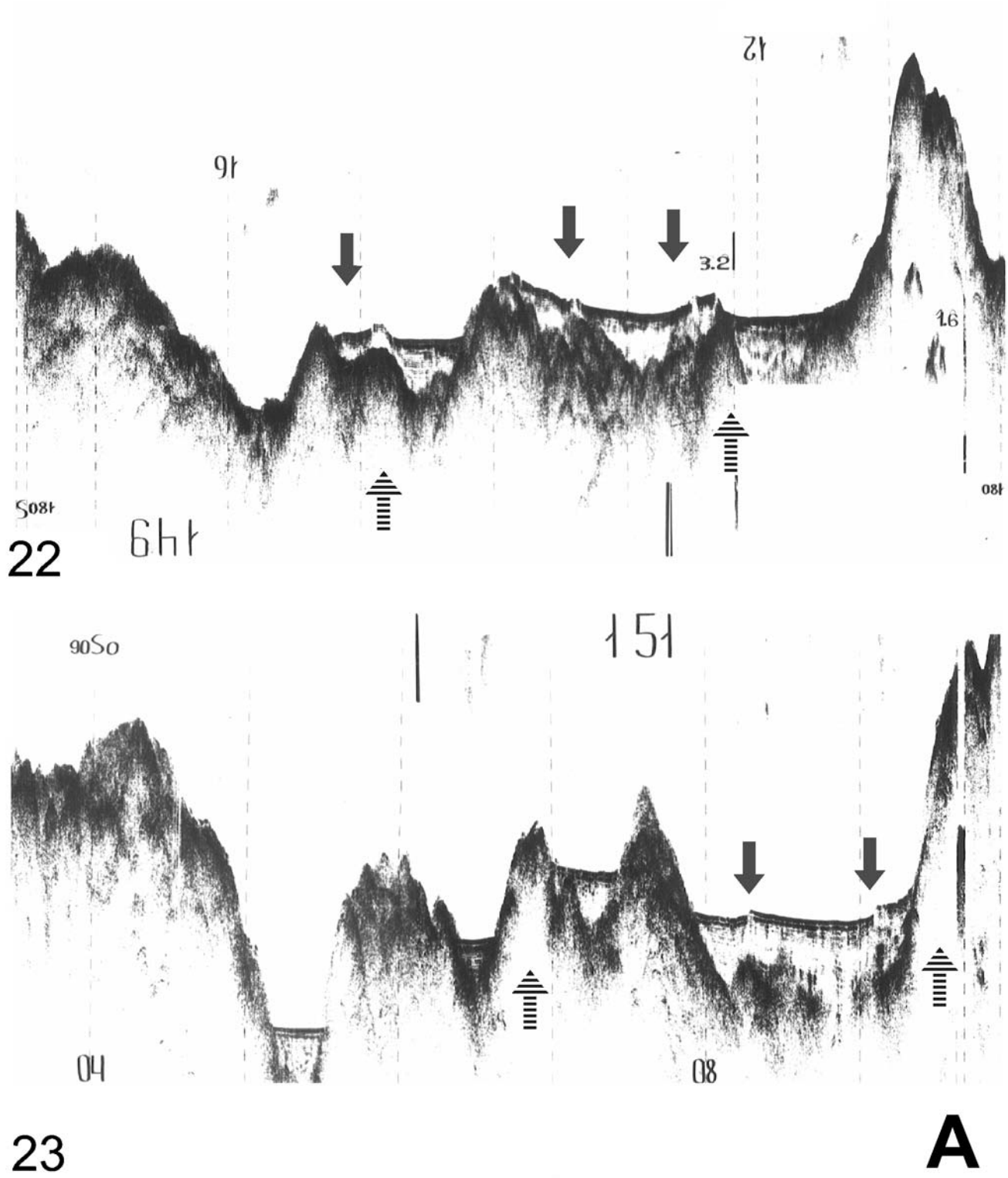

Figure 13. Continuous seismic profiles. For location, see Figure 3. Red arrows indicate examples of deformation and blue arrows, possible areas of acoustic basement uplift. a – Seismic profiles 22–23.

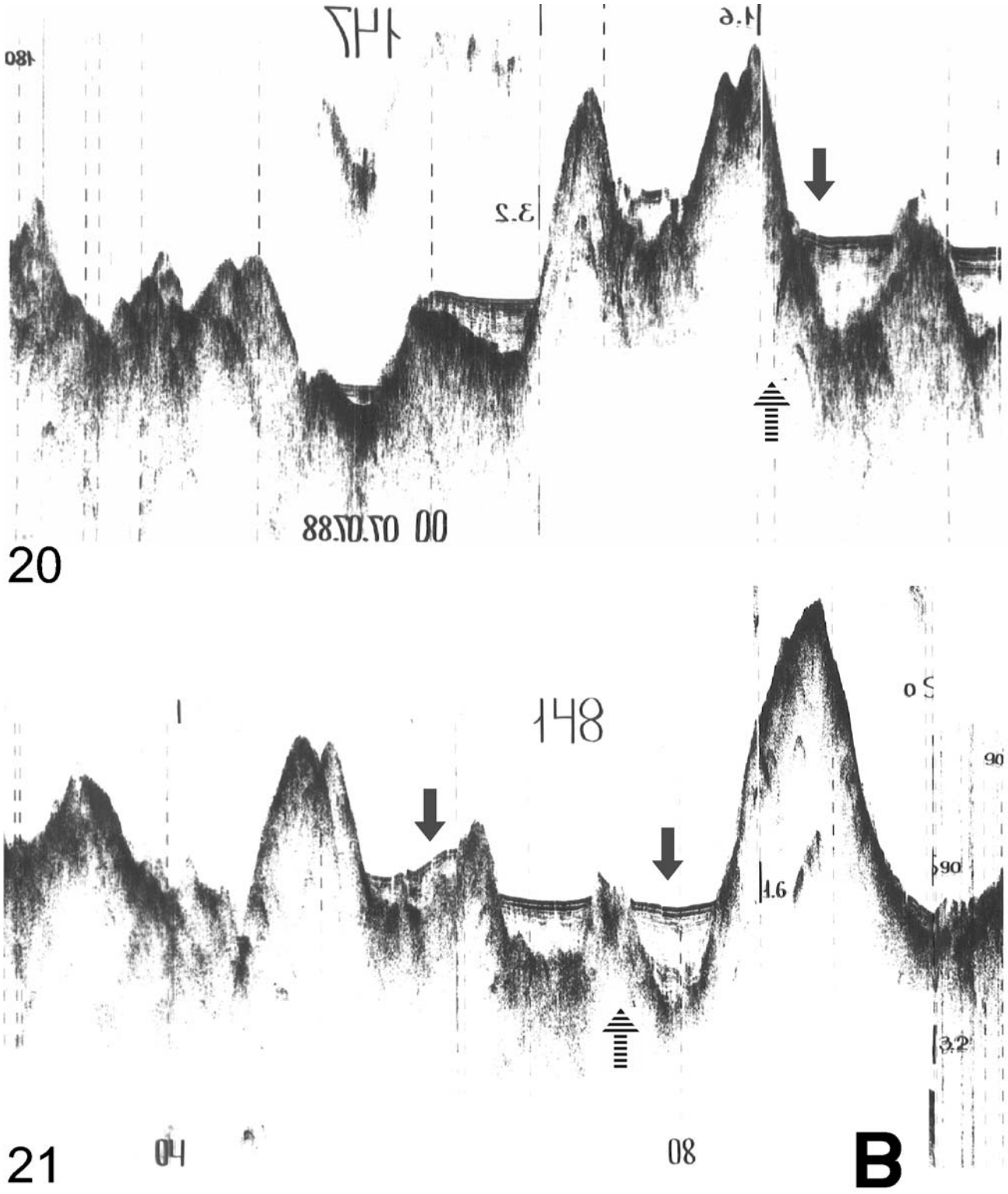

Figure 13. Continuation. b – Seismic profiles 20–21.

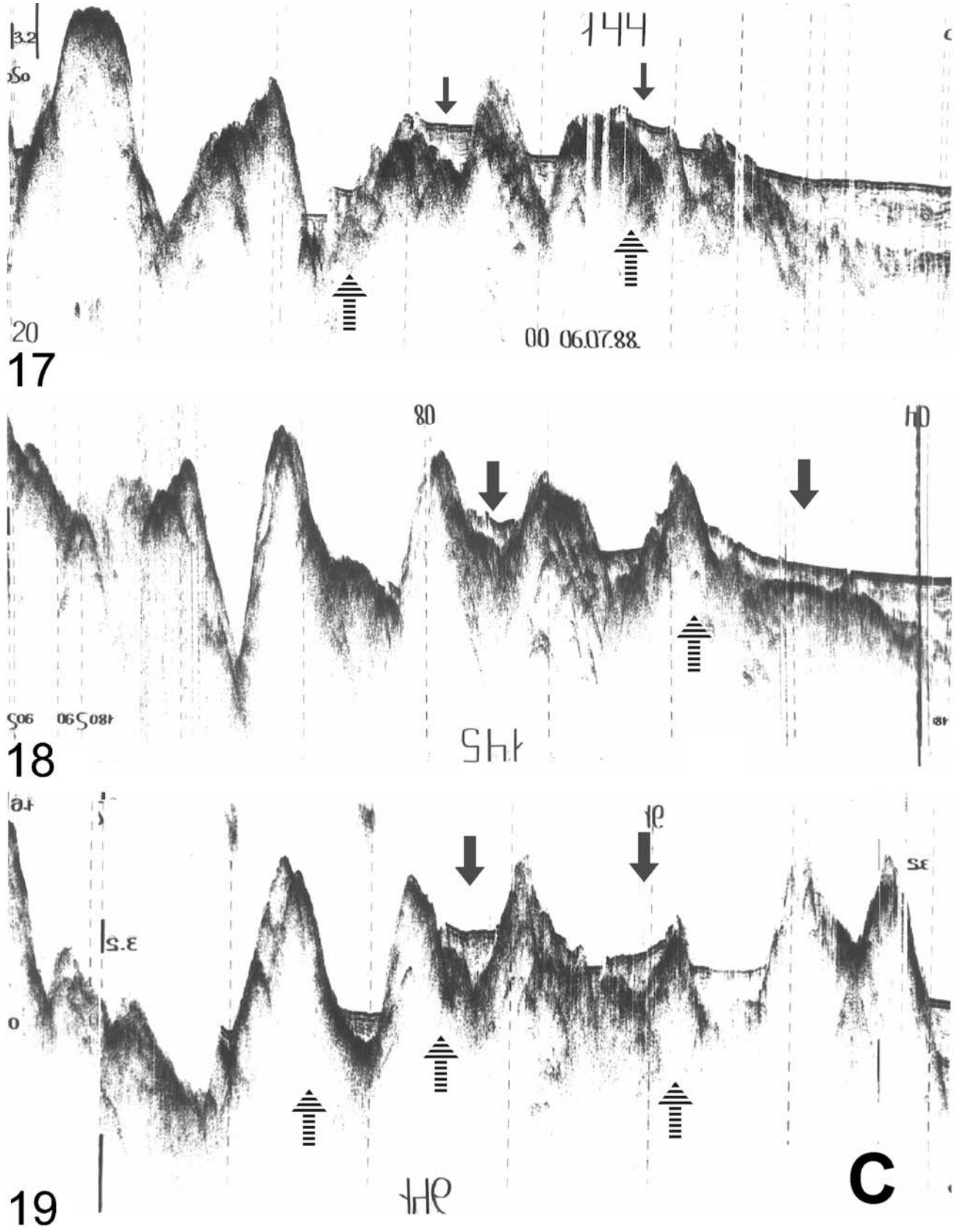

Figure 13. Continuation. c – Seismic profiles 17–19.

nately, the area remains as yet undredged, and it thus is not possible to correlate slope angles to rock types. Seismically, this part of the ridge is most active.

The eastern part of the ridge has a considerably different structure. This part occurs in average water depths of 3500 m. Against this topographic environment, numerous variously oriented mountains over 1000 m high and hills 200–400 m high stand out. This topographic pattern resembles serpentinite melange terranes onshore. The area was explored by two successful dredge hauls (Figure 11) and submersible operations. On the R/V Akademik Nikolaj Strakhov Cruise 7, dredge S0732D recovered serpentinized harzburgite and altered basalt and, on Cruise 22, dredge S2227D sampled talcite, peridotite, and gabbro. Submersible operations in the area of the nodal basin revealed the presence of a broad rock spectrum ranging from basalt to serpentinized ultramafite [*R. Hekinian,* personal communication, May 17, 2000]. This area is aseismic. To summarize, our analysis of assorted data reveals considerable structural heterogeneities along the inter-fracture ridge, a circumstance suggestive of drastic changes in the geodynamic setup of the entire region through time.

The SP3-4_RI rift zone (25°25′ W) is a narrow (in places, up to 2 km), short (10–12 km) gorge with symmetrical walls and a stripe of flat-bottomed basins along its axis. The rift valley walls have angles of 5–8° but, with increasing distance from the rift axis, slope angles become steeper, in places up to 30°. Dredge hauls and the dives of the French submersible in the interior of the rift valley revealed widely occurring basalts with fresh glasses [*R. Hekinian,* personal communication, May 17, 2000]. The valley walls are composed of a broad spectrum of oceanic crustal rocks with a large proportion of ultramafites displaying various degrees of serpentinization. To the north, the rift gorge passes into a large nodal basin with slopes 12–15° steep, although here (e.g., on the northern slope) both areas with steeper angles and flat tracts are present. The basin has a triangular shape and is elongated along the **SP3** fracture. To the southeast, no nodal basin is present but, at the southwestern end of the rift, a small sediment-filled depression lies. On trend with the rift valley, a 100 to 150-m-high scarp occurs. It extends across the **SP3** fracture and continues further as a narrow curvilinear valley. At the intersection, a small depression is situated. Some distance south, a large flat-topped mountain stands out, which has a gentle northwestern slope and whose slopes become steeper toward the top. Here, a dredge haul from the R/v Robert Conrad [*Schilling et al.,* 1995] recovered basalt with fresh glasses. The general aspect of the mountain and the dredged rocks suggest that, virtually on trend with the **SP2-3_RI** rift zone, a large volcanic edifice is situated. This inference is not inconsistent with the large positive Bouguer anomalies (Figure 9b).

The SP3-4_E_RI ridge throughout its length is virtually devoid of sediment (Figure 7). Immediately east of the **SP2-3_RI** rift valley, this ridge represents a mountainous massif with a mesa-like surface, whose structure is modified by several hills and seafloor depressions. The ridge has average slope angles of 3 to 12°, although in places these are as great as 15° and, occasionally, up to 30°.

The SP4 trough is a depression in acoustic basement, which, west of the rift valley, shows a sedimentary fill as thick as 400 or 500 m, reaching 800 m in the western part of the trough. The trough bottom lies in average water depths of 4000 m. A bathymetric map with a 10 m contour interval resolves a seafloor pattern of alternating elongate basins, not infrequently bent in plan view, with intervening benches or topographic scarps. In individual basins, depths are as great as 4100 or 4150 m. The trough also hosts several hills of isometric shape. Two of these, the most conspicuous, have distinctive structures. One is cone-shaped and stands ca. 100 m high against the surrounding topography, while the other has two tops on a single base. Its total height is over 200 m. The slope angles are in places as great as 10°. It is noteworthy that, just as in the **SP4** fault, several thresholds are distinctly recognized that bar the whole width of the trough (Figure 5). They stand out as high as 100 m. The eastern part of the trough, coinciding with the active segment of the fracture zone, has very steep, up to 45°, walls. Here, sedimentary cover is virtually unrecorded.

The SP4-5_RI rift zone (25°W) extends 34 km within the study area, and its northern part is ca. 4 km wide. Its bottom lies in water depths of 4050 to 4100 m. Along the

Table 2. Virtual geographic names within the São Paulo survey area (from north to south)

Feature	Symbol
Fault depressions	
São Paulo 1 (northernmost fault)	SP1
São Paulo 2	SP2
São Paulo 3	SP3
São Paulo 4 (southernmost fault)	SP4
Inter-fracture ridges	
Between faults SP1 and SP2 east of the rift	SP1-2_E_RI
Between faults SP2 and SP3 west of the rift	SP2-3_W_RI
Between faults SP3 and SP4 west of the rift	SP3-4_W_RI
Between faults SP1 and SP2 east of the rift	SP1-2_E_RI
Between faults SP2 and SP3 east of the rift	SP2-3_E_RI
Between faults SP3 and SP4 east of the rift	SP3-4_E_RI
Rift zones	RI
Between faults SP2 and SP3	SP2-3_RI
Between faults SP3 and SP4	SP3-4_RI
Between faults SP4 and SP5	SP4-5_RI
Nodal basins	NB
Fault SP2, eastern	NB_SP2_E
Fault SP3, western	NB_SP3_W
Fault SP3, eastern	NB_SP3_E

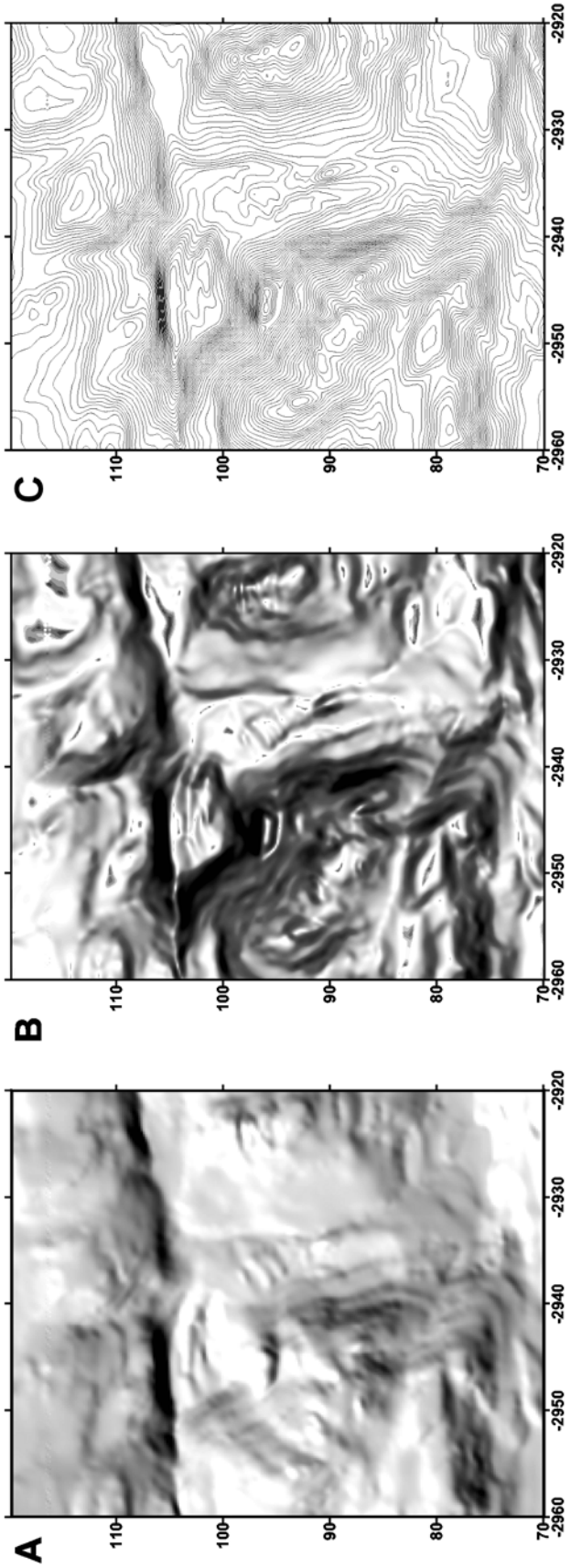

Figure 14. Detailed maps showing the SP2-3_RI rift zone (26°25'W): a - bathymetric map constructed using the shaded relief technique; b - map showing slope angles; c - bathymetric map with a 50-m contour interval. Projection coordinates.

axis of the rift, basins lie whose bottom surfaces have angles of 0 to 3°. To the south, as a scarp is crossed, the rift valley widens abruptly to 13 km. The southern segment shows a complex topographic pattern with a number of rises elongated roughly N-S. These have intricate contours in plan view and horizontal top surfaces. Near the threshold, on which slope angles are as great as 15°, an isometric rise occurs, whose base is ca. 3 km in diameter and ca. 300 m in height, and which most likely represents a central-type volcanic edifice. Its slopes have angles of 12–15°, and its top is flat.

In addition to the features just described, the northern and southern boundaries of the fractures are established in the survey area. These boundaries have been covered by surveys only fragmentarily. The southernmost trough is an acoustic basement depression filled with sediments as thick as 400–500 m. The troughs bottom lies in water depths of 4000 m. A bathymetric map with 10 m contour interval resolves a seafloor pattern of alternating elongate basins, often bent in plan view, separated by sills or scarps, and several isometric hills. Judging from satellite altimetry data (Figure 9), these basins are complexly built seafloor areas. Topographically, the southern boundary is expressed as an elevated "plateau" with steep slopes, modified by a number of roughly N-S trending valleys. On the north, large mountains or ridges with extremely steep slopes are situated. The Belousov Seamount, in the northeastern part of the survey area, is featured by a negative Bouguer anomaly suggestive of low-density constituent lithologies, such as serpentinized rock masses or vesicular and, consequently, density-deficient volcanites. This inference is supported by dredge hauls from the R/V Akademik Boris Petrov (BP1701-BP170), which recovered serpentinized ultramafite, breccia, and basalt. Judging from satellite altimetry data, the seamount is the westernmost part of a large ridge.

Along the northern margin of the fracture zone, a zone of active sedimentation extends **(SP1_FZ)**, which corresponds to a nearly horizontal seafloor area. Sedimentary cover there is underlain by a deep acoustic basement depression with a wide and flat bottom (Figure 8).

Seismic Signature of the Active Segment of the São Paulo FZ

Between 1950 and 1997, 55 earthquakes ranging in magnitude from 3.0 to 6.7 were recorded in the study area [*CNSS...*, 1997]. The number of subcrustal (13 to 35 km deep) quakes was 23 and of crustal (0 to 13 km deep), 32. Plotted over the topography (Figure 10), these data show that only three quakes, one in each rift valley, were recorded in the rift zones proper. Furthermore, of those foci located in the rift, the one in the northern part of the valley, at 26°25′ W, falls virtually within the trough, and the one at 25°30′ W, in the southernmost part on the western wall. The only within-rift focus falling in the valley interior was located at 25°W. Its projection is located on the transverse sill separating the rift valley into the northern and southern segments. The earthquakes took place in 1969, 1975, and 1976, their magnitudes equaling 4, 5, and 5 and their depths, 33, 10, and 33 km, respectively. In the active segments of the fracture zones, a total of three 10-km-deep earthquakes were recorded, all falling between the first and second rifts (in 1986, 1997, 1996), with magnitudes of 5, 4, and 4, respectively.

For 15 quakes recorded within the survey area, fault-plane solutions were calculated, which are available in the Harvard University Catalog [*Harvard...*, 1997]. The study of the focal mechanisms (Figure 10) reveals displacements of the "normal fault" type in the rift zone and of the "strike-slip" type along the fault troughs but, unlike those oceanic fracture zones in which the vector of motion on the fault plane is directed longitudinally, this survey area displays strike slips whose vectors point roughly N-S. This suggests the presence in the crust of a strong N-S stress component, which is released in faulting along all the shear directions theoretically possible with respect to the stress axis.

The majority of earthquakes, however, are concentrated in the southwest of the survey area. Note that seismicity is strongest in the area of steep slopes of the **SP3-4** and **SP2-3** inter-fracture ridges. The **SP4_FZ** zone (the western, passive part) is aseismic but, as the rift is approached, 30–40 km from it an earthquake cluster is recorded. In the western passive part of the **SP3_FZ**, M = 5 quakes are confined to the most submerged portions of the trough. The depth of the foci is 33 km in the west and 10 km in the east.

Discussion

The above materials demonstrate that computer processing of the data acquired twelve years ago renders a wealth of new information amenable to a geological analysis that enables the architecture of the active segment of the São Paulo Fracture Zone to be reinterpreted in a largely innovative manner.

In the study area, several tectonic zones with distinctive structures were delineated: rift zones and active portions of the faults, terranes bordering the fracture zone, and a tract of thick sedimentary cover showing evidence of several deformational phases. In addition, superimposed features represented by volcanic edifices were discovered.

In the rift zones and active portions of the transform faults, sedimentary cover is virtually absent and mountainous relief with slope angles exceeding 20° prevails. All the rift zones show distinctive inner structures and modes of junction with the faults. Two rift zones, **SP2-3_RI** and **SP3-4_RI**, are located inside the São Paulo fault system, and **SP4-5_RI** is developed in the transition from the multiple fault system to its bordering terrane. The former displays all the constituents of a classical oceanic rift – asymmetrical walls and a well pronounced rift-valley bottom surmounted by a neovolcanic ridge. The ridge extends into the confines of the northern nodal basin, likely suggesting an extension zone propagating into the active segment of the **SP2_FZ**. The northern part of the rift valley is cut by a set of NE-trending faults. To the south, the neovolcanic ridge

bends westward – i.e., toward the passive part of the fault. The southern nodal basin is divided by a sill into two cells displaced one with respect to the other, a pattern not inconsistent with the existence of a NW-trending fault with some amount of strike slip. The **SP3-4_RI** rift valley has symmetrical gently sloping walls and a narrow bottom. To the north, a large triangular nodal basin, and to the south, a topographic scarp is located, which not only crosses the fault trough, but also offsets all the topographic features after the fashion of a sinistral shear. The **SP4-SP5_RI** rift zone consists of two segments, and its topography increases in complexity in the direction of the wall rocks. The set of within-rift ridges and volcanic edifices testify that this tectonic feature is evolving actively. No nodal basin has been detected at the rift-fault junction.

A zone of extensively developed sedimentary cover is located north of $1^{\circ}10'$ N. In addition, the entire eastern, passive part of the **SP2_FZ** can be attributed to this zone. This whole area represents a combination of accumulative sedimentary bodies and a relict or newly formed relief. Overall, it is located within the São Paulo FZ. The analysis of 23 continuous seismic profiles shows a broad spectrum of deformations involving sediments of various types and ages. The fact that deformation in the sediments increases in magnitude from normal faults in the east to flexures and homoclines in the west might suggest that the ridge is propagating eastward. A variety of causes may be proposed to account for this extraordinary phenomenon, the most likely being the dramatic seafloor uplift in the vicinity of the São Pedro e São Paulo Rocks, located northwest of the survey area.

Therefore, the vigorous tectonic activity characterizing the study area goes beyond the scope of a mere extension in rift zones or strike-slip displacements along the active portions of transform faults. It is noteworthy that, alongside E-W trending features, the topographic grain of the study area displays a clear northwesterly trend manifest in the elongation of undersea mountains, direction of valleys, and arrangement of depositional zones. The most likely underlying cause might be a system of right-lateral strike slips of the same trend. This is not inconsistent with the presence of slip vectors directed roughly N-S (Figure 10). These faults control the distribution of sediment thicknesses, which are especially great (600 to 1100 m) in depocentral areas, indicating rather old ages for the inception of these faults.

Secondly, the study area provides the setting for the formation of major volcanic edifices. Two of these are located on trend with the rift valleys. This interpretation is supported by both the pattern of gravity anomalies and, in a number of cases, by dredging results.

Our study shows that converting information from paper carriers to a digital format and combining the results with Internet resources and deep sea sampling data creates an entirely new dataset amenable to state-of-the-art processing techniques eventually leading to unexpected corollaries.

This work is a step toward the creation of a GIS that would allow an expeditious analysis of the structure of the region in question, and it outlines the basic approaches to be used in this context over the entire Atlantic.

Acknowledgment. This work was carried out in the framework of the Research in the Nature of the World Ocean subprogram of the World Ocean Specialized Federal Program implemented by the Russian Federation Ministry of Science and Industry.

References

Agapova, G. V., Features of the offset morphology of the São Paulo Fracture Zones, *Oceanology, 34,* (1), 107–112, 1994.

CNSS Earthquake Composite Catalog, June 1997, (http://quake.geo.berkeley.edu/cnss/).

Gorini, M. A., The Tectonic Fabric of the Equatorial Atlantic and Adjoining Continental Margins: Gulf of Guinea to Northeastern Brazil, *Serie Projecto,* (9), 111 pp., 1981.

Harvard University Centroid-Moment Tensor Catalog, December 1997, (http://www.seismology.harvard.edu/CMTsearch.html).

Marine Trackline Geophysical Data CD, NOAA Product No. G01321-CDR-A0001.

Sandwell, D. T., and W. H. F. Smith, Marine Gravity Anomaly from Geosat and ERS-1 Satellite Altimetry, *J. Geophys. Res., 102,* (B5), 10,039–10,054, 1997.

Smith, W. H. F., and D. T. Sandwell, Global seafloor topography from satellite altimetry and ship depth soundings, *Science, 277* (5334), Sept. 26, 1997.

Schilling, J.-G., C. Ruppel, A. N. Davis, B. McCully, S. A. Tighe, R. M. Kingsley, and J. Lin, Thermal structure of the mantle beneath the equatorial Mid-Atlantic Ridge: Influence from the spatial variation of dredged basalt glass compositions, *J. Geophys. Res., 100,* (B7), 10,057–10,076, 1995.

The Equatorial Segment of the Mid-Atlantic Ridge, appendix to the monograph The Equatorial Segment of the Mid-Atlantic Ridge, 33 pp., IOC UNESCO, GEOKhI RAS, ATKAR PKO Kartografiya, 1997.

(Received July 19, 2001)